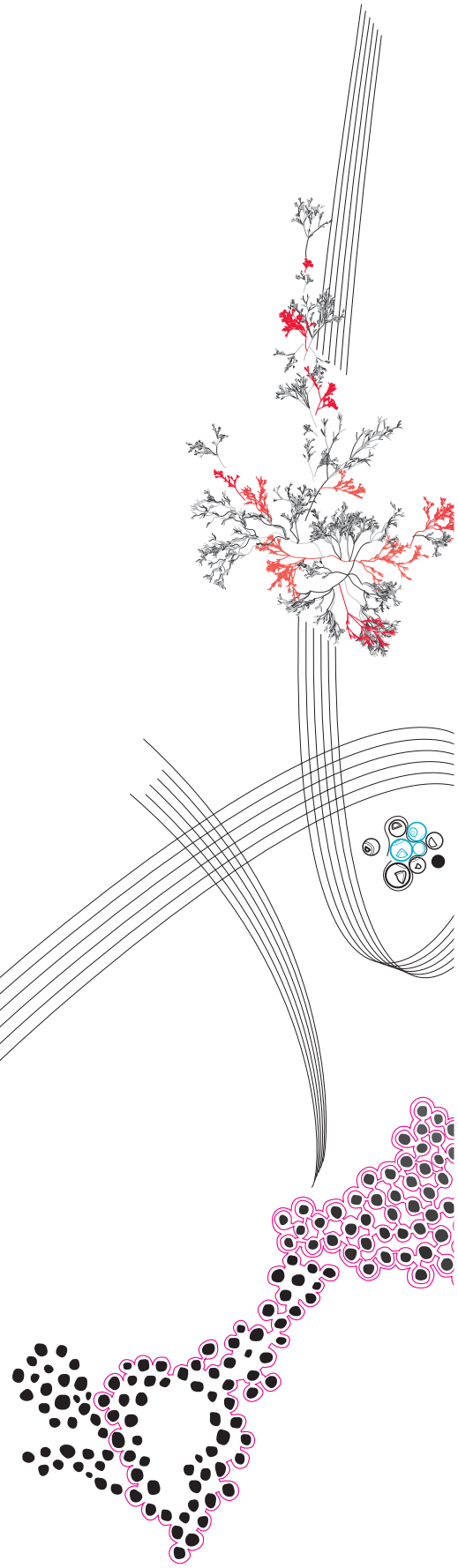

BSc Thesis Applied Mathematics

The Influence of Spike-Timing Dependent Plasticity on Synaptic Connectivity of Coupled Inhibitory Neurons

Sem Jani Geerts

Supervisor: Dr. H.G.E. Meijer (Hil)

June, 2019

Department of Applied Mathematics
Faculty of Electrical Engineering,
Mathematics and Computer Science

UNIVERSITY OF TWENTE.

Preface

This paper is written as a final thesis for the Bachelor of Science in Applied Mathematics at the University of Twente.

Twenty weeks ago, this project started with my choice for this specific subject, as it was one of the few titles I did not understand for a single bit. Twenty weeks later, I am proud to say I do, and have never had such a steep learning curve in my life. This paper is the report of this project, and with it, my first three years at university will come to an end. In truth, I could not have achieved my current level of success without a strong support group.

I have gained lots of insight in this topic in discussions with friends, family and fellow students. Trying to explain something to someone that has not read many research papers on the topic proved to be challenging, and showed me many aspects of missing knowledge on my part. Specifically, I would like to thank my parents for always being enthusiastic and thoughtful. Also, much love to Anne for being able to deal with me for so long, thank you for being understanding and motivating all these years.

Furthermore, I would like to thank my supervisor Dr. H.G.E. Meijer for his great advice and tutoring during this project. He knew very well how to push and excite me for the next step, even though often unclear. The long meetings we held were great for showing me there was much to learn. Hil could give direction in one sentence without ever giving the exact solution, and shared my excitement for new results.

All in all, I enjoyed the process where I saw various seemingly disparate courses of by bachelors coming together in one final project.

I hope you enjoy your reading.

Sem

June 28th, 2019

The Influence of Spike-Timing Dependent Plasticity on Synaptic Connectivity of Coupled Inhibitory Neurons

Sem J. Geerts*

June, 2019

Abstract

Inhibitory neurons exist throughout the brain, and many brain nuclei function inhibitory on other nuclei as well, some involved in diseases such as Parkinson's disease. Investigating the coupling of these neurons might lead to new insight for developing techniques such as deep brain stimulation further. The effect of spike-timing-dependent plasticity (STDP) is studied on a leaky integrate-and-fire model to characterise the final weight configurations. To simplify analysis, a sinusoidal-coupled phase-difference model is investigated. The framework of STDP is reformulated as phase-difference-dependent plasticity (PDDP) to study multiplicative learning rules. Moreover, weight dynamics is analysed using phase averages. The aim is to study the effect of two main parameters, the strength of additive noise and the difference in intrinsic frequency on the synaptic connectivity. It is concluded that large noise induces stable bidirectional coupling. Bistability of unidirectional coupling and weak bidirectional coupling is observed in the phase-difference model. Moreover, increasing the intrinsic frequency difference interchanges the type of unidirectional coupling for small additive noise. Typically, in both models we observe decoupling of the neurons to be unstable, therfore, neurons will never decouple but synchronise in firing frequency. Stable firing patterns are only observed for large synaptic weight values compared to detuning frequency.

Keywords: firing patterns, LIF, PDDP, phase-difference, STDP, weight stability

1 Introduction

The brain consists of many neurons, which can be coupled in several forms. We distinguish both excitatory and inhibitory neurons. The former describes neurons that stimulate each other to fire. When two excitatory neurons are coupled and one produces an action potential, the other neuron will fire sooner. Inhibitory neurons show the opposite behaviour, where neurons are inhibited by one another and reduce each other's firing frequency.

Another characteristic of neurons is called plasticity, which enables humans to learn [4]. Neurons are coupled with a certain coupling-strengths, which determine the amount of influence one neuron has on another. These weights can change over time, and the amount of influence (the coupling-strength) will change due to influence of the firing patters of the neurons. Moreover, there are several ways neurons interact and are coupled, which is called synaptic connectivity and is described by the values of synaptic weights. With unidirectional coupling, we refer to the case where one neuron does influence the other, but not conversely. In bidirectional coupling, both neurons can influence each other. When two

*Email: s.j.geerts@student.utwente.nl

neurons do not impact each other at all, it is called decoupling. The way coupling weights change over time and are updated under the influence of different system characteristics is called plasticity.

Spike-timing dependent plasticity (STDP) is a one specific type of plasticity that describes how the coupling of two neurons is affected by the neuron's firing activity, it is a fundamental adaptation mechanism which induces structural changes in synaptic connectivity [3]. This is described by a certain learning rule, where the change of coupling weights depends on the time difference between two firing spikes, resulting in an update function at discrete time points. The influence of STDP on firing patterns and synaptic connectivity of excitatory neurons has been investigated by [3], they modelled two coupled neurons as noise-enhanced oscillators. Noise is essential in their research, as neuronal behaviour is constantly under influence of natural fluctuations and external coupling with other neurons. They have shown that for some parameter values, multi-stability of different coupling configurations (synaptic connectivity) is possible. Moreover, bidirectional coupling was shown not to be possible in the noise-free situation, but this could be induced by noise. Therefore, increased noise can synchronise neurons with different natural firing frequencies. This is summarised in Figure 1. In this figure, $\Delta\omega$ denotes the difference in natural frequency, and μ the noise intensity. Red indicates stable unidirectional coupling, blue indicates stable bidirectional coupling. Decoupling was stable for all parameter values. For large values of $\Delta\omega$, i.e. for significantly de-synchronised neurons, bidirectional coupling cannot be achieved anymore.

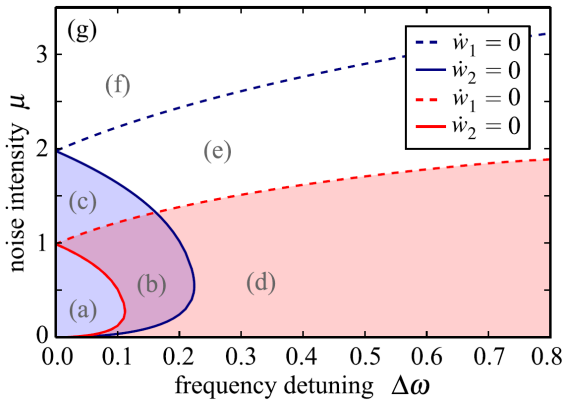

FIGURE 1: Bifurcation diagram for excitatory neurons by Lücken et al. [3].

STDP can come in several forms, which depends on the type of neuron we are dealing with, as well as the location within the brain [3, 5]. The main distinction that can be made is the additive and multiplicative learning rule. In the former, weights are updated with a given amount, irrespective of their initial values and only dependent on the spike-timing difference, while in the latter, weights are updated with respect to their initial value as well. Here the relative update is constant for the a given spike-timing difference [7, 8]. The results obtained by [3] were found by using additive rules for excitatory neurons. We will concern ourselves with multiplicative rules for inhibitory neurons.

Inhibitory neurons are present in almost every part of our central nerve system. One brain region specifically is called the external globus pallidus (GPe), which is (almost) exclusively inhibitory, and plays an important role in the reduction of symptoms of Parkinson's disease using deep brain stimulation (DBS) [6, 11]. We will model two coupled neurons in the GPe which forms a subset of an important system in the coupling with the Subthalamic nucleus (STN), where DBS is applied which relieves some of the symptoms of

Parkinson's disease [10]. Modelling this part of these two brain cores will give more insight in its working and potential efficiency of DBS.

This is done by first looking at a simple integrate-and-fire model for two coupled inhibitory neurons and determine the regular firing patterns and stable phase differences of the spikes. We then implement STDP learning rules for inhibitory neurons and determine its influence on the firing patterns, weight dynamics and stability. Furthermore, we will analyse a phase-difference model, where the framework of STDP will be re-written to a phase-difference-dependent plasticity (PDDP), which simplifies analysis. In a noise-induced system, stable phase differences and the stability of certain weight configurations can be investigated. The goal is to find which model parameters induce stability of the different types of synaptic connectivity, and what influence that has on firing patterns.

2 Leaky Integrate and Fire Model

The simplest model describing the dynamics of a spiking neuron is the so-called leaky integrate-and-fire (LIF) model. The general differential equation is given by

$$C\frac{dV}{dt} = V_r - V + RI(t),$$

where C is the capacity of the membrane, V_r the resting potential and $I(t)$ some external input that is applied. This model is a differential equation where in the absence of input $I(t)$ we get that $V(t) \to V_r$. The value of V is reset to a certain value $V_I = 0$ when a certain threshold V_θ is reached, which we take this value to be $V_\theta = 1$. When $V = V_\theta$, a spike occurs. In general, $V_r < V_\theta$, as the opposite would mean a constant natural firing of a neuron, where we only want neurons to fire when the external input $I(t)$ is large enough to induce a spike.

2.1 Coupled neurons

In a system of two coupled neurons, the input $I(t)$ depends on the firing of the other neuron. Since the variables can be scaled, we choose $C = 1$ and let $I_i(t) = RI(t) + V_r$ be the sum of resting potential and external input, which yields the system of equations

$$\begin{cases} \dfrac{dV_1}{dt} = -V_1 + I_1(t), \\ \dfrac{dV_2}{dt} = -V_2 + I_2(t). \end{cases} \tag{1}$$

The input I_j depends on the firing times of other neurons. For inhibitory neurons, we have that when neuron i fires at time τ_i, the input of other neurons $j \neq i$ gets updated with

$$I_j(t) \to I_j(t) - I_{s,j}(t - \tau_i), \tag{2}$$

where $I_{s,j}$ is the contribution coming from the spike of the action potential. The minus sign ensures that an action potential in neuron i inhibits neuron $j \neq i$, characteristic for inhibitory neurons. In this case we choose to take the α-function

$$I_{s,j}(t) = \begin{cases} w_j \cdot \varrho\alpha^2 t e^{-\alpha t} & \text{for } t > 0, \\ 0 & \text{otherwise,} \end{cases}$$

where the value of w_j determines the strength of the coupling of the firing of the neurons, ϱ determines the overall maximum strength of the influence, and the parameter $\alpha > 0$

determines the duration of the spike influence and ensure that the overall input integrated over time is equal to $w_j \varrho$:

$$\int_{-\infty}^{\infty} I_{s,j}(t)dt = \left[-w_j \varrho \alpha t e^{-\alpha t}\right]_0^{\infty} + \int_0^{\infty} w_j \varrho \alpha e^{-\alpha t} dt = \left[-w_j \varrho e^{-\alpha t}\right]_0^{\infty} = w_j \varrho.$$

We choose to let the synaptic weights be bounded by $0 \leq w_j \leq w_{max} = 1$. In general, we can write the input functions $I_{1,2}(t)$ as

$$\begin{cases} I_1(t) = I_1 + \sum\limits_{t>\tau_{2,k}} w_1(\tau_{2,k}) \varrho \alpha^2 (t - \tau_{2,k}) e^{-\alpha(t-\tau_{2,k})}, \\ I_2(t) = I_2 + \sum\limits_{t>\tau_{1,k}} w_2(\tau_{1,k}) \varrho \alpha^2 (t - \tau_{1,k}) e^{-\alpha(t-\tau_{1,k})}, \end{cases} \tag{3}$$

where again $\tau_{i,k}$ denotes the k-th firing of neuron i. Note that the value of the weights is variable over time, as will be discussed in Section 2.2. Moreover, the weight term is dependent on the times of firing $\tau_{i,k}$, rather than on the real time t. This is done as the α-function behaves decreases fast between two spikes. Therefore, when weights are updated again, the value of $I_{s,i}$ is practically zero. This choice drastically simplifies numerical computations.

We choose to have $I_1, I_2 > 1$, such that, without the external input of the coupling ($\varrho = 0$), both neurons are always naturally firing with a natural frequency. This frequency can be calculated, as the differential equation can be solved for $\varrho = 0$. Both inputs are in that case constant, i.e. $I_i(t) = I_i$ for both neurons, solving yields

$$\begin{cases} V_1(t) = I_1 + (V_1(0) - I_1)e^{-t}, \\ V_2(t) = I_2 + (V_2(0) - I_2)e^{-t}. \end{cases}$$

A neuron fires when it reaches $V_i(t_\theta) = V_\theta$ first. This happens for

$$\begin{aligned} V_i(t_\theta) =& I_i + (V_i(0) - I_i)e^{-t_\theta} = V_\theta \\ \rightarrow \quad & t_\theta = \ln\left(\frac{I_i - V_i(0)}{I_i - V_\theta}\right). \end{aligned}$$

Since we fixed V_θ, the duration between two spikes can be calculated, which is equivalent to t_θ when $V_i(0) = 0$. We define the natural period T_i and maximal period T of the two neurons to be equal to

$$T_i := \ln\left(\frac{I_i}{I_i - 1}\right), \quad \text{with } T := \max\{T_1, T_2\}. \tag{4}$$

The natural firing frequency is then equal to $\Omega_i := 2\pi/T_i$.

2.2 Spike-Timing Dependent Plasticity

The synaptic weights w_i are not constant over time but vary and can change due to several influences. The way these weights behave and change over time is called plasticity. We will introduce one form of plasticity for inhibitory neurons which will be extensively investigated.

We will focus on spike-timing dependent plasticity (STDP), which implies that the change of weights depends on the time of firing between the two respective neurons. This

difference in firing is denoted as $\Delta t := t_{post} - t_{pre}$, where t_{post} and t_{pre} are the times of firing of the post-synaptic and pre-synaptic neurons respectively. From the perspective of neuron 1, $\Delta t > 0$ implies that neuron 2 just fired which gives extra input to neuron 1 (when $w_1 > 0$). On the contrary, in the case of $\Delta t < 0$, neuron 1 has just created an action potential and inhibits neuron 2. An extra input is given to neuron 2 and $t_{pre} > t_{post}$. Hence, in general for two coupled neurons, when one neuron observes a spike-timing difference of Δt, the other neuron observes a spike-timing difference of $-\Delta t$.

We can distinguish two types of STDP rules, additive and multiplicative [7, 8]. Both are update functions of the weights dependent on this time difference Δt. An update rule of the additive type can be written in the form

$$w_i \to w_i + \delta \Delta w_i(\Delta t), \tag{5}$$

where δ denotes the weight update strength and Δw_i incorporates the Δt dependence in neuron i as a learning rule. In general, we choose the learning rules to be the same for both neurons. A multiplicative STDP rule is written in the form

$$w_i \to w_i \cdot \Gamma_{w_i}(\Delta t),$$

where Γ_{w_i} denotes the learning rule of neuron i. Note that in the multiplicative rule, there is no update strength δ involved. When it is desired to scale this function, this should be done inside the learning rule Γ_{w_i}.

Additive STDP rules are often used as scaling is done more easily due to the external scaling parameter δ. The dynamics can then be directly influenced in the weight update itself. However, in experimental studies that have tried measuring STDP rules of brain neurons, multiplicative rules are often obtained. Therefore, for the remainder of this paper we will solely focus on multiplicative STDP rules.

2.3 Learning Rules

In general, learning rules for multiplicative STDP can be written in the form

$$\Gamma_w(\Delta t) = \begin{cases} \Gamma_{w_+}(\Delta t) & \text{for } \Delta t > 0, \\ \Gamma_{w_-}(\Delta t) & \text{for } \Delta t < 0, \\ 1 & \text{for } \Delta t = 0. \end{cases} \tag{6}$$

In excitatory neurons the largest updates are being done for small Δt, while in inhibitory neurons, for Δt near zero, very little change in synaptic strength is observed [1]. Therefore, the last case for $\Delta t = 0$ is included as fixed rule in Equation 6. Using 78 neurons, Haas et al. have obtained the data that can be seen in Figure 2(a).

Fitting this data has resulted in the following learning rule

$$\Gamma_w(\Delta t) = \begin{cases} \Gamma_{w_-}(\Delta t) = 1 + \beta_- \, (\Delta t)^{10} \, e^{\alpha_- \Delta t}/n, & \text{for } \Delta t < 0 \\ \Gamma_{w_+}(\Delta t) = 1 + \beta_+ \, (\Delta t)^{10} \, e^{\alpha_+ \Delta t}/n, & \text{for } \Delta t > 0 \quad [5] \\ 1 & \text{for } \Delta t = 0, \end{cases} \tag{7}$$

with $\beta_- = -2.60 \cdot 10^{-7}$, $\beta_+ = 2.29 \cdot 10^{-6}$ and $\alpha_- = 0.94$, $\alpha_+ = -1.10$. Here n is described as the number required to induce the synaptic change per unit time [5], and is assumed to be equal to 1. This parameter can be seen as the scaling parameter that is missing in the general form of the multiplicative update rule, increasing n will decrease the update size.

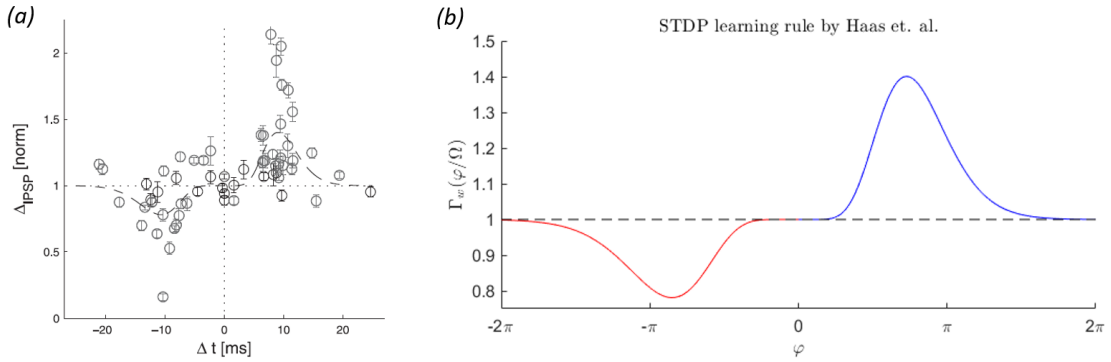

FIGURE 2: (a) Fitted data for inhibitory STDP learning rule [1]. (b) Multiplicative learning rule for inhibitory neurons as general function of phase difference φ.

The original experiment performed by [1] had a maximum duration of $T = 25$ ms between firings, as can be seen in Figure 2(a). Therefore, we use a natural spiking frequency $\Omega := 2\pi/T = 2\pi/25\ \text{ms}^{-1}$, which is necessary to scale other frequencies to the same learning rule. The neurons of the LIF model do not necessarily have the same natural period T. To accommodate for this fact, the spike-timing difference Δt can also be written as a phase difference $\varphi \in (-2\pi, 2\pi)$ using the linear mapping $\mathcal{F}$, where $\varphi = \mathcal{F}(\Delta t) := 2\pi\Delta t/T$. This only holds with the assumption that Δt does not exceed the maximum period T, therefore an alternating firing pattern is required. In this way, the learning rule in Equation 7 can be generalised with $\Gamma_w(\varphi/\Omega)$, for all natural frequencies Ω with corresponding maximal period T. This yields the function as in Figure 2(b), where the update Γ_w is plotted as a function of phase difference.

2.4 Influence of STDP on Synaptic Connectivity

In this section, we look at the influence of spike-timing dependent plasticity on stable weight configurations and eventual synaptic connectivity. We use the system of Equations 1 with input function Equation 3, with $\alpha = 2$, as then coupling-spike will be smaller than the natural period T_i.

A mostly alternating firing pattern (1-2-1-2-1- etc.) is desired, otherwise complete suppression of one neuron would take place. To achieve this, the maximum coupling influence is set to $\varrho = 0.3$. Larger values (e.g. 0.4) will lead to de-synchronisation of the firings, or complete suppression of neuron 1, see Figure 20 in Appendix A. Smaller values (e.g. 0.15) will resemble decoupling, where the influence is so little that it can not be noticed anymore and neurons simply follow their natural frequency, see Figure 21 in Appendix A. For initial conditions we choose $V_1(0) = 0$, $V_2(0) = 0.5$, and $w_1(0) = w_2(0) = 0.2$ as significantly larger values of the weights will result in immediate suppression of neuron 1 due to high a high value of the first input function.

Neuron 2 has initial input $I_2 = 1.40$, while the input for neuron 1 is variable between $I_1 \in [1.15, 1.40]$. Both constant inputs are larger than 1 to induce constant firing in a decoupled state. Smaller values for I_1 will lead to complete suppression. Weights are updated according to learning rule in Equation 7, with $n = 1$. To scale the learning rule accordingly, the maximum period T of the natural firing frequencies is used as in Equation 4. The phase difference can be written as $\varphi = 2\pi\Delta t/T$, and we use the update $\Gamma_w(25\Delta t/T)$, to compensate for the shift in natural period from 25 ms to T ms in the original learning rule.

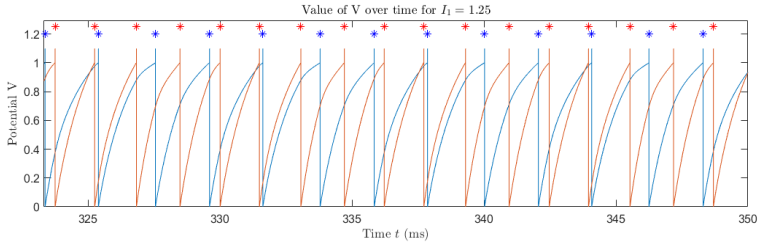

FIGURE 3: Example of membrane potential with $\alpha = 2, \varrho = 0.3$ for the last part of a 350 ms run

Membrane potentials over time for both neurons can be seen in Figure 3, simulated using the Euler method, with indicated firing times. The constant input for neuron 1 is equal to $I_1 = 1.25$, smaller than that of neuron 2, which results in a smaller frequency. In approximation, the firing pattern is still alternating, something necessary for further analysis.

In Figure 4, the weight values over time can be seen corresponding to the simulation of Figure 3. Even though both weights start at 0.2, it can be seen that they both converge to a stable pattern after 50 ms.

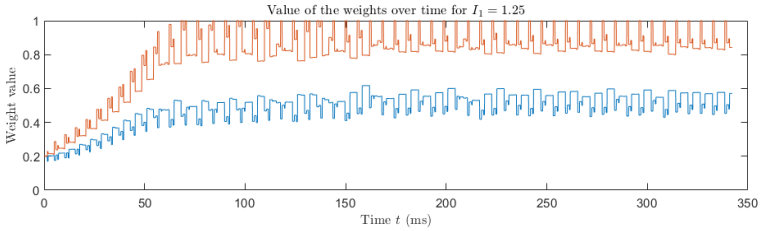

FIGURE 4: Example of weight values with $\alpha = 2, \varrho = 0.3$ for a 350 ms run. The weight values are updated with every spike and clearly stabilise.

The difference in input $\Delta I := I_2 - I_1 \in [0, 0.25]$ is used to induce a difference in natural firing frequency, as seen in Figure 3. We determine the average value of the weights for the last part of a long run (i.e. the final convergence as seen in Figure 4), and look at the influence of the input difference ΔI. This can be seen in Figure 5.

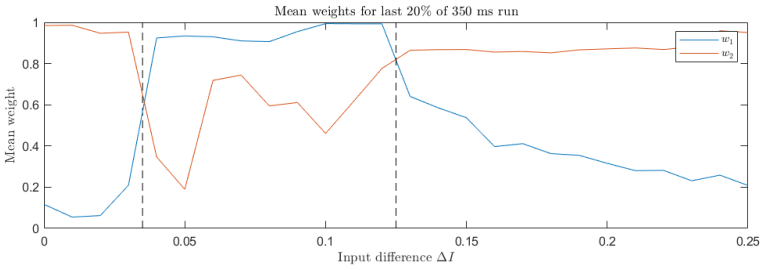

FIGURE 5: Average weights after a long run as a function of input difference ΔI, with $\varrho = 0.3, w_1(0) = w_2(0) = 0.2$.

Note the three intervals for which unidirectional and weak bidirectional coupling is stable. The intervals of types of synaptic connectivity separated by the values $\Delta I = 0.035$ and $\Delta I = 0.125$. These results show the dependency of the synaptic connectivity on the natural frequency difference, induced by ΔI, and are highly dependent on other parameter

values. Changing ϱ as an immediate effect on the location of certain synaptic connectivity ranges, as can be seen in Figure 22 in Appendix A.

2.4.1 Addition of Noise

The model previously presented is relatively simplified as it only models the interaction of two neurons and eliminates all external natural perturbations. One important notion is that the system is connected to many other neurons also influencing the change of membrane potential via additional input. This is introduced using additional random input in the form of additive noise with intensity σ and independent Wiener processes W_i. The system of equations is equal to

$$\begin{cases} dV_1 = (-V_1 + I_1(t))\,dt + \sigma dW_1, \\ dV_2 = (-V_2 + I_2(t))\,dt + \sigma dW_2, \end{cases}$$

where the input I_i is still described by the neuron coupling in Equation 3. This is numerically implemented using the Euler-Maruyama scheme as provided in Equation 21 in Appendix B. Using the numerical simulation, the average (converging) value of the weights can be obtained. This is done for the last 20% of the simulation, as an initial period to achieve a stable state is necessary and a small initial condition should not be taken into account. For simulations where $\sigma \neq 0$, six runs are performed, of which the average weight values are used.

The initial weight conditions are chosen to be $w_1(0) = w_2(0) = 0.2$, as larger values can again lead in complete suppression of neuron 2 from the beginning onward. No weight updates will take place in these cases, therefore, larger initial values are neglected. The noise intensity varies in the range of $\mu \in [0, 0.03]$, larger values will lead to chaotic and decoupled behaviour, where the influence of noise greatly exceeds the influence of the coupled input function in Equation 3.

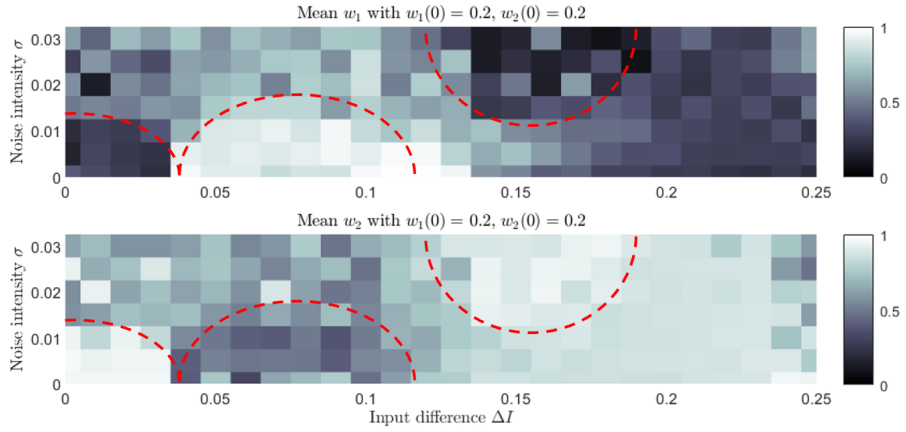

FIGURE 6: Average weight values for the last 20% of a 350 ms run, with $\alpha = 2$, $\varrho = 0.3$, and indicated regions where (weak) unidirectional coupling is visible.

The results of these simulations can be seen in Figure 6. Note how the bottom row is equal to the values that can be seen in Figure 5. We can distinguish certain areas in this plot. For $\Delta I < 0.04$, and small noise intensity, there is a strong unidirectional coupling, with $(w_1, w_2) \approx (0, 1)$, also recognised in Figure 5. In the range $0.04 < \Delta I < 0.12$, there appears to also exist unidirectional coupling, although not as strong with $(w_1, w_2) \approx$

$(1, 0.4)$. For larger noise and larger ΔI, we have another region where weak unidirectional coupling exists $(w_1, w_2) \approx (0.2, 0.9)$.

For larger values of noise, and for $\Delta I > 0.23$, we observe that results become less clear and distinct. In these cases, noise influences the natural firing pattern significantly, and natural frequencies differ too much. In conclusion, it is clear that analysis of this system is hard to perform and largely dependent on chosen model parameters. Results are highly subject to noise and numerical simulations, as becomes clear from Figure 6. Therefore, we will move to a phase difference model, which will be discussed in the next section.

3 Phase Model

A simple model for a pair of mutually coupled neurons will be analysed in this section. We consider two phase oscillators $\vartheta_1(t)$ and $\vartheta_2(t)$ with natural firing frequencies of ω_1 and ω_2. The coupling weights of the neurons are w_1 and w_2, where the first belongs to the incoming action potential for neuron 1 as in Figure 7. The neurons have a certain natural frequency, and the phase $\vartheta_i \in [0, 2\pi)$ describes the state the neuron is in and the moment of the next firing. A neuron fires when its phase reaches $\vartheta_i \to 2\pi$, after which it is reset to 0. The model is then given by two ordinary differential equations as

$$\begin{cases} \dfrac{d\vartheta_1}{dt} = \omega_1 + w_1 g(\vartheta_2 - \vartheta_1), \\ \dfrac{d\vartheta_2}{dt} = \omega_2 + w_2 g(\vartheta_1 - \vartheta_2). \end{cases}$$

Here g is a 2π-periodic function describing the interaction of the two neurons as a function of the phase difference. The coupling is the same for both neurons even though $\omega_1 \neq \omega_2$. Natural fluctuations are introduced in the form of additive noise by an independent Wiener processes W_1 and W_2, which act on the dynamics with intensity $\sqrt{\mu}$. The model is then described by the following two stochastic differential equations

$$\begin{cases} d\vartheta_1 = (\omega_1 + w_1 g(\vartheta_2 - \vartheta_1))\, dt + \sqrt{\mu} dW_1, \\ d\vartheta_2 = (\omega_2 + w_2 g(\vartheta_1 - \vartheta_2))\, dt + \sqrt{\mu} dW_2. \end{cases}$$

This system can also be written as a single stochastic differential equation. We do this by defining the phase difference of the two neurons $\varphi(t) := \vartheta_2(t) - \vartheta_1(t)$. Note that this phase difference is also restricted to the interval $[0, 2\pi)$. The evolution of φ is given by the stochastic differential equation

$$d\varphi = (\Delta\omega + w_2 g(-\varphi) - w_1 g(\varphi))dt + \sqrt{2\mu} dW. \tag{8}$$

Here $\Delta\omega = \omega_2 - \omega_1 > 0$ is the difference of the intrinsic frequencies, and $W = (W_2 - W_1)/\sqrt{2}$. Since W_1 and W_2 are independent random variables both normally distributed, $W(t) \sim N(0, t)$ is again an independent Wiener process. We choose sinusoidal coupling with $g(\varphi) = \sin(\varphi)$.

3.1 From STDP to phase-dependent plasticity

As mentioned in Section 2.2, the weights can change over time due to STDP, and are updated according to a learning rule. The goal is to find which types of synaptic connectivity are stable under the influence of noise μ and the intrinsic frequency difference $\Delta\omega$. The STDP as stated in Section 2.2 could be implemented numerically, however, for analysis

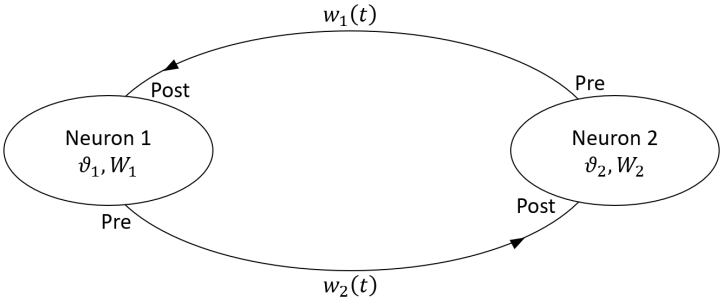

FIGURE 7: Schematic representation of two coupled neurons.

it turns out to be be easier to transform this discontinuous STDP (which only updates at times a spike occurs), to a continuous learning rule that is dependent on a continuous variable. We will transform this into a Phase-Difference-Dependent Plasticity (PDDP) [3]. In this case the change of weight $\dot{w}$ is a function P of the phase difference φ, hence

$$\dot{w}_i = P_i(\varphi(t)) \tag{9}$$

Lücken et. al. have transformed the additive STDP as in Equation 5 into a PDDP rule [3]. We concern ourselves with multiplicative STDP, and will construct this approximation of the continuous PDDP rule for multiplicative STDP learning rules. The general form of a multiplicative learning rule is used as in Equation 6.

To transform this time-difference dependent update function into a phase-continuous approximation in PDDP form, we will look at what happens during a time interval dt on average, and start with only looking at neuron 1 (ϑ_1) with corresponding weight w_1. With Ω we denote the average spiking frequency, or the frequency of the locked state. Then $\Omega/2\pi$ equals the average number of firings per unit time. When looking at the weight a timestep dt further, we can write this as a function of the initial weight $w_1(t)$. During an interval dt, the average number of spikes of neuron 1 is equal to $dt \cdot \Omega/2\pi$. Therefore, we can write the weight at the next time step as

$$w_1(t + dt) \approx w_1(t) \cdot (\Gamma_{w_1})^{dt\Omega/2\pi},$$

where Γ_{w_1} is the true overall update of weight 1 between two firings of the postsynaptic neuron of neuron 1. We need to determine the overall weight update Γ_{w_1}. The spikes of neurons 1 and 2 are sketched in Figure 8. The red bars indicate the times neuron 1 fires, the times t where $\vartheta(t) = 0$. Similarly, the blue bars indicate a spike of neuron 2.

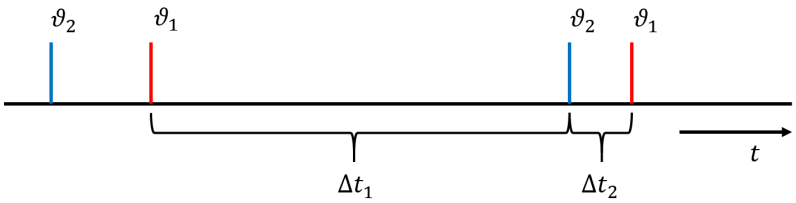

FIGURE 8: Schematic representation of the twofold weight update between two spikes of ϑ_1.

It is assumed that between two firings of the post-synaptic neuron 1 (red lines), the presynaptic neuron 1 has also received an action potential, such that two updates occur, with absolute spike-timing differences Δt_1 and Δt_2. This assumption is only valid for

relative small detuning frequency $\Delta\omega/\Omega$. Van Vreeswijk et. al. have shown that inhibition causes synchronisation of firing patterns for some coupling mechanisms [9]. Therefore the assumption of alternating firing patterns can be justified for small $\Delta\omega$. Now from the perspective of neuron 1, the respective updates are $\Gamma_{w_-}(-\Delta t_1)$ and $\Gamma_{w_+}(\Delta t_2)$. Due to the multiplicative nature of the STDP rule, these two updates should be multiplied to obtain the overall weight update Γ_{w_1} happening between two postsynaptic spikes. Hence we get the twofold update

$$w_1(t+dt) \approx w_1(t) \cdot \left(\Gamma_{w_+}(\Delta t_2) \cdot \Gamma_{w_-}(-\Delta t_1)\right)^{dt\Omega/2\pi}.$$

However, as stated above, we require phase-dependency to obtain a weight differential equation in the PDDP form of Equation 9. We proceed by using the average spiking frequency Ω, and by first looking at Δt_2.

When the postsynaptic neuron 1 fires, i.e. $\vartheta_1 = 0$, we have that $\varphi = \vartheta_2$. Since Ω is the frequency of the locked state, and thus also the frequency between two spikes of neuron 2, we have $\Delta t_2 = \vartheta_2/\Omega = \varphi/\Omega$. Since the time between two firings of the postsynaptic membrane is equal to $2\pi/\Omega$, we get that $\Delta t_1 = 2\pi/\Omega - \Delta t_2$, resulting in $-\Delta t_1 = (\varphi - 2\pi)/\Omega$. Now that spike-timing differences can be approximated by the phase difference of the two neurons, the STDP rule can be written as a PDDP rule. Using the definition of the derivative, we derive an ordinary differential equation for the weight update.

$$\frac{dw_1(t)}{dt} \approx \frac{\Omega}{2\pi}\left[\ln\left(\Gamma_{w_+}\left(\frac{\varphi}{\Omega}\right)\right) + \ln\left(\Gamma_{w_-}\left(\frac{\varphi - 2\pi}{\Omega}\right)\right)\right] w_1(t).$$

The full derivation can be found in Equation 19 in Appendix B. The roles of $\Delta t_{1,2}$ are interchanged for neuron 2, with $w_2(t+dt) \approx w_2(t) \cdot \left(\Gamma_{w_+}(\Delta t_1) \cdot \Gamma_{w_-}(-\Delta t_2)\right)^{dt\Omega/2\pi}$. Hence, the PDDP transformation for w_2 can be directly determined (see Equation 20 in Appendix B). Overall, this results in the system of weight dynamics

$$\begin{cases} \dot{w_1}(t) = w_1(t)q(\varphi), & \text{for } 0 \leq w_1 < w_{max}, \\ \dot{w_2}(t) = w_2(t)q(2\pi - \varphi), & \text{for } 0 \leq w_2 < w_{max}, \end{cases} \tag{10}$$

where

$$q(\varphi) := \frac{\Omega}{2\pi}\left[\ln\left(\Gamma_{w_+}\left(\frac{\varphi}{\Omega}\right)\right) + \ln\left(\Gamma_{w_-}\left(\frac{\varphi - 2\pi}{\Omega}\right)\right)\right], \quad \text{for } \varphi \in [0, 2\pi). \tag{11}$$

Weights cannot exceed the maximum weight w_{max}, so the weight dynamics should be limited on the boundaries. We do this by forcing hard bounds on the boundaries, where

$$\begin{cases} \dot{w_1}(t) = \min(w_1(t)q(\varphi), 0), & \text{for } w_1 = w_{max}, \\ \dot{w_2}(t) = \min(w_2(t)q(2\pi - \varphi), 0), & \text{for } w_2 = w_{max}. \end{cases}$$

Forcing hard bounds on the minimum $w_i = 0$ is not necessary, as weights can only be zero if and only if $w_i(0) = 0$, as can be seen from Equation 10. With the value $\Omega = 2\pi/25$ ms^{-1}, we obtain the continuous phase update function as described in Equation 11 using the learning rule from Equation 7, shown in Figure 9.

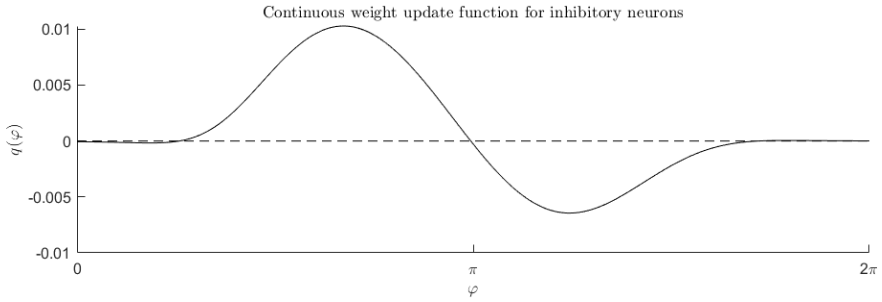

FIGURE 9: Continuous weight update function for inhibitory neurons using PDDP.

3.2 Numerical Simulations

The phase model of Equation 8 with weight update functions as in Equations 10 and 11 is numerically implemented such that results can be analysed, which gives more insight in the stability of weights. Simulations are run using the numerical scheme as provided in Equation 22 in Appendix B.

Several model parameters determine the behaviour of the weights and phase difference, which will quickly be discussed. Both stable and unstable phase differences are visible, but the phase difference φ will quickly converge to a stable configuration around $\varphi = 0$ when possible. Due to this fact, the phase difference is plotted on the interval $[-\pi, \pi)$, which makes visualisation of the periodic and stable phase difference more clear.

The weight evolution depends on several parameters. Firstly the weights' initial values. This is illustrated in Figure 10 with relatively little noise ($\mu = 0.01$).

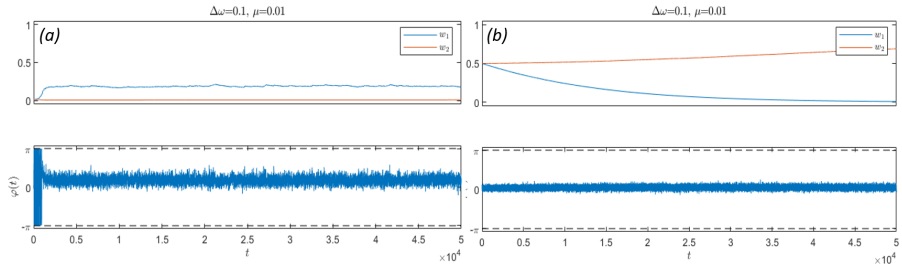

FIGURE 10: Numerical simulations with $\Delta\omega = 0.1, \mu = 0.01$. Note the dependency of weight- and phase difference dynamics on the initial conditions: (a) Initial conditions $w_1(0) = w_2(0) = 0.01$. (b) Initial conditions $w_1(0) = w_2(0) = 0.5$.

From Figure 10 it appears that there are multiple stable weight configurations the pair of weights can converge and stabilise into. These stable configurations can only be reached form certain initial conditions. The value of the weights not only influences the eventual stable phase difference φ^*, but also the size of the fluctuations, even though the noise intensity remains the same. When the phase difference stabilises, neuronal firing is synchronised and fixed (or oscillating due to noise) in a certain pattern.

The influence of larger values of noise is mostly trivial and can be seen in Figure 23 in Appendix A. A simulation with large $\Delta\omega$ can be seen in Figure 11(b). Here, the phase difference φ does not oscillate around a fixed value, but remains constantly increasing (on average). In this case, an alternating firing pattern is not reached, as one neuron 1 ($\Delta\omega > 0$) is always trailing behind. Therefore, for large values of $\Delta\omega > 0$, stable firing patterns are never attained. In general, we can also conclude, that the weights converge relatively slowly into a stable configuration, while the phase difference can remain unstable.

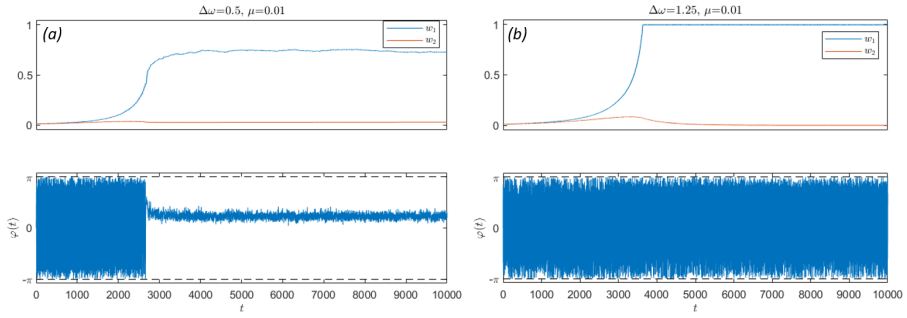

FIGURE 11: Numerical simulations with $\mu = 0.01$ and $w_1(0) = w_2(0) = 0.01$. Note the dependency of weight- and phase difference dynamics on the value of the difference in intrinsic frequency: (a) $\Delta\omega = 0.5$. (b) $\Delta\omega = 1.25$.

3.3 Phase Dynamics, Stability and Firing Patterns

For fixed weights and in the absence of noise ($\mu = 0$), the governing differential equation in Equation 8 can be solved analytically. Obtaining these solutions for fixed weights is a valid approximation, as the dynamics of the phase difference is much faster than that of the weights as seen in Section 3.2.

3.3.1 Stable Solution

Firstly, we look at the stable converging states that might exist for sinusoidal coupling, where all initial conditions of φ will converge to. Let $\nu(\varphi) := d\varphi/dt = \Delta\omega - w_1 \sin(\varphi) + w_2 \sin(-\varphi)$ define this ordinary differential equation in the absence of noise. The critical points are then found by finding the roots of $\nu(\varphi)$, which are equal to

$$\begin{aligned} &\nu(\varphi) = \Delta\omega - w_1 \sin(\varphi^*) + w_2 \sin(-\varphi^*) = 0 \\ \rightarrow \quad &\varphi_1^* = \arcsin\left(\frac{\Delta\omega}{w_1 + w_2}\right), \quad \varphi_2^* = \pi - \arcsin\left(\frac{\Delta\omega}{w_1 + w_2}\right). \end{aligned}$$

These solutions only exists for $(w_1 + w_2) \geq \Delta\omega$. For stability of these critical points it is desired that $\nu'(\varphi_i^*) < 0$, which only holds for $\varphi^* := \varphi_1^*$. When noise is introduced ($\mu > 0$) and weights remain fixed, the phase difference φ will still converge to this stable solution and fluctuate around it due to noise disturbances. Having a stable solution of the phase difference implies having a stable firing pattern, where the difference in spike-times remains fixed ($\vartheta_2 - \vartheta_1 = \varphi^*$); two coupled inhibitory neurons will synchronise.

3.3.2 Periodic Solution

When $(w_1 + w_2) < \Delta\omega$, no stable phase difference exists as the equation $\nu(\varphi) = 0$ can not be solved. However, a periodic solution does exist, which we will obtain for $\mu = 0$. We do this by solving our differential equation $\nu(\varphi) = \varphi'(t)$ on the interval $[-\pi, \pi)$[1], i.e.

$$\varphi'(t) = \Delta\omega - (w_1 + w_2)\sin(\varphi(t)), \quad \varphi(0) = -\pi.$$

By separating variables and integrating, we get

$$-\frac{2}{\sqrt{\Delta\omega^2 - w^2}} \arctan\left(\frac{\Delta\omega - w\tan(\varphi/2)}{\sqrt{\Delta\omega^2 - w^2}}\right) = t + c_1, \tag{12}$$

[1]Solving on this interval simplifies analysis . Since we are dealing with phases, the range $[-\pi, \pi)$ is equivalent to the range $[0, 2\pi)$

where $w := w_1 + w_2$. Rewriting yields the phase function

$$\varphi(t) = 2\arctan\left(\frac{1}{\Delta\omega}\left[w - \gamma\tan\left(\frac{\gamma}{2}(c_1 - t)\right)\right]\right), \tag{13}$$

where $\gamma := \sqrt{\Delta\omega^2 - w^2}$. This turns out to be a periodic function, and we are interested in the periodicity τ of the variable φ, such that $\varphi(t+\tau) = \varphi(t)$ (for later purposes mostly). This is equivalent to finding τ with $\lim_{t\to\tau}\varphi(t) = \pi$, since $\varphi(0) = -\pi$.

We first determine the value of integration constant c_1. Substituting our initial value in Equation 12 and taking the limit[2] yields

$$c_1 = \lim_{t\downarrow 0} t + c_1 = \lim_{\varphi\downarrow -\pi} -\frac{2}{\gamma}\arctan\left(\frac{\Delta\omega - w\tan(\varphi/2)}{\gamma}\right) = -\frac{\pi}{\gamma}.$$

This approach can also be extended to find our value for τ, where we obtain

$$\lim_{t\uparrow\tau} t + c_1 = \lim_{\varphi\uparrow\pi} -\frac{2}{\gamma}\arctan\left(\frac{\Delta\omega - w\tan(\varphi/2)}{\gamma}\right) = \frac{\pi}{\gamma}.$$

Hence, we get that the duration of one full cycle is equal to $\tau = 2\pi/\gamma$. Again, this solution is only in the absence of noise. For $\mu > 0$ this solution is still an approximation and the true value will fluctuate around this solution. Having a periodic solution implies that the phase difference φ is constantly increasing on the interval $[0, 2\pi)$. Therefore, ϑ_2 constantly increases faster than ϑ_1, and the two neurons do not synchronise; neuron 1 is constantly lagging behind.

3.4 Weight Dynamics and Stability

There is a mutual dependency of the phase difference φ and the weight values as described by Equations 8 and 10. However, as stated before, in Section 3.2 it can be seen that the evolution of the phase difference is much faster than that of the weights. Therefore, we can determine the overall behaviour of the weights based on the time-averaged behaviour of the phase difference. In this section we want to determine this phase-averaged behaviour of synaptic weights so that stable weight configurations can be determined.

3.4.1 Phase-Averaged Weight Dynamics

Since we are dealing with noise-induced dynamics with stochastic differential equations for the phase difference φ, and want to obtain phase-averaged weight dynamics, a phase distribution is necessary. For this, we let ρ be the probability density function (pdf) of the phase φ. The phase difference φ does converge to a stable distribution when this exists, but will always continue to fluctuate around this value when noise is introduced. Again, we are dealing with the stochastic differential equation

$$d\varphi = \nu(\varphi)dt + \sqrt{2\mu}dW.$$

Since W is an independent Wiener process, the probability density function ρ follows the Fokker-Planck equation (FPE), which is the partial differential equation

$$\frac{d\rho}{dt} = -\frac{d}{d\varphi}\left(\nu(\varphi)\rho\right) + \mu\frac{d^2\rho}{d\varphi^2}. \tag{14}$$

[2]Since the inverse tangent (like in Equation 13) never truly reaches $\pm\pi/2$, but only approaches it as the inside goes to $\pm\infty$, we have to take the limit.

We assume that the pdf converges to some stationary distribution $\rho_s := \lim_{t\to\infty} \rho$. As the phase difference φ behaves much faster than the dynamics of the weights w, we can approximate the weight dynamics using ρ_s, by taking the weighted average over the phase difference interval with

$$\begin{cases} \dot{w_1} = w_1 \int_0^{2\pi} q(\varphi)\rho_s(\varphi)d\varphi, \\ \dot{w_2} = w_2 \int_0^{2\pi} q(2\pi-\varphi)\rho_s(\varphi)d\varphi, \end{cases} \tag{15}$$

where the stationary pdf ρ_s is a function of φ, and depends on weights w_1, w_2, noise intensity μ, and intrinsic frequency difference $\Delta\omega$. These last two values are chosen to be constant and we use the $2\pi-$periodic function $g(\varphi) = \sin(\varphi)$. Note that the weights now are not dependent on the value of φ, as this is integrated out, but only dependent on its distribution. By using the stationary pdf ρ_s, this function is independent of time.

3.4.2 Weight Dynamics without Noise

We will first describe the weight dynamics in the absence of noise, as all derivations can be done analytically. Even though the use of a probability density function (as in the Fokker-Planck equation) is not necessary in this case, it can still be used to describe the dynamics.

a) In the case $(\mathbf{w_1} + \mathbf{w_2}) \geq \boldsymbol{\Delta\omega}$, a stable solution for φ exists. The phase difference will reach the stable state φ^* relatively fast compared to the change of weights. Hence, we assume that the phase difference will be precisely equal to this stable state. In that case, ρ_s will be equal to the Dirac delta function

$$\rho_s(\varphi|w_1, w_2) = \delta(\varphi - \varphi^*).$$

This results in our phase-averaged dynamics for the synaptic weights with

$$\mu = 0 \text{ and } (w_1 + w_2) \geq \Delta\omega \rightarrow \begin{cases} \dot{w_1} = w_1 q\left(\arcsin\left(\dfrac{\Delta\omega}{w_1+w_2}\right)\right), \\ \dot{w_2} = w_2 q\left(2\pi - \arcsin\left(\dfrac{\Delta\omega}{w_1+w_2}\right)\right). \end{cases}$$

b) In the case $(\mathbf{w_1} + \mathbf{w_2}) < \boldsymbol{\Delta\omega}$, no stable phase difference exists. However, we can still characterise the dynamics of the weights, as the value of $\varphi(t)$ is known by Equation 13. Therefore, the distribution ρ_0 can be determined as well. This is done by observing that the probability that the phase difference φ is below some value X is equal to

$$\mathbb{P}(-\pi \leq \varphi \leq X) = \frac{T(\varphi(t) = X)}{\tau},$$

where $T(\varphi(t) = X) \in [0, \tau)$ denotes the time at which the phase difference is equal to the value $X \in [-\pi, \pi)$ for the first time. Hence, T is a function of X and actually the inverse function of φ, this can be seen in Figure 12. Using Equation 12 we can directly obtain this inverse function and

$$T(X) = \varphi^{-1}(X) = \frac{\pi}{\gamma} - \frac{2}{\gamma}\arctan\left(\frac{\Delta\omega - w\tan(X/2)}{\gamma}\right).$$

Hence, on the interval $[-\pi, \pi)$, we have that

$$\begin{aligned}\rho_0(\varphi) &:= \frac{d}{d\varphi}T(\varphi)/\tau = \frac{d}{d\varphi}\left[\frac{1}{2} - \frac{1}{\pi}\arctan\left(\frac{\Delta\omega - w\tan(\varphi/2)}{\gamma}\right)\right] \\ &= \frac{w}{2\pi\gamma\cos^2(\varphi/2)}\frac{1}{((\Delta\omega - w\tan(\varphi/2))/\gamma)^2 + 1}.\end{aligned}$$

Due to the 2π-periodicity[3] of the function ρ_0, we have that $\rho_0(\varphi - 2\pi) = \rho_0(\varphi)$ for all φ. Hence, our system of equation can be written into its original form as in Equation 15, meaning

$$\mu = 0 \text{ and } (w_1 + w_2) < \Delta\omega \rightarrow \begin{cases} \dot{w_1} = w_1 \int_0^{2\pi} \rho_0(\varphi) q(\varphi) d\varphi, \\ \dot{w_2} = w_2 \int_0^{2\pi} \rho_0(\varphi) q(2\pi - \varphi) d\varphi. \end{cases}$$

Note in Figures 12(a-b) how steeper the function $\varphi(t)$, the lower the probability is, as the time duration of the phase difference existing in that specific interval is smaller.

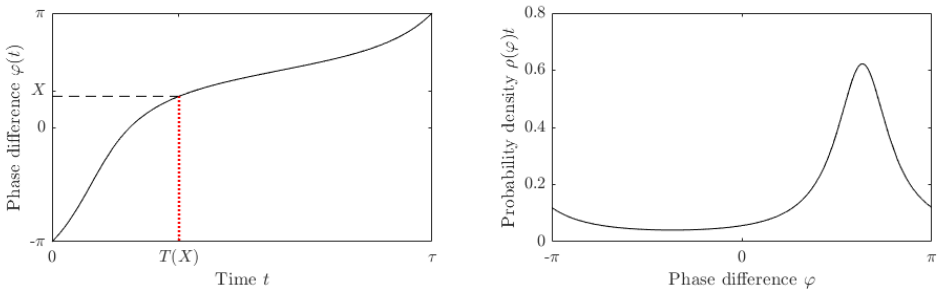

FIGURE 12: $w = 0.1, \Delta\omega = 0.2$ (a) Example of phase difference $\varphi(t)$ with location of $T(X)$. (b) Steady state probability distribution function ρ_s on $[-\pi, \pi)$.

3.4.3 Weight Nullclines

From numerical simulations it can be seen that phase difference stabilises if that value can be attained. Since the stable phase difference φ^* is known, we can look at the dynamics of the weights to determine for which values these will be stationary. For w_1, stability is reached when

$$\begin{aligned} & w_1 q(\varphi_1^*) = w_1 \frac{1}{2\pi}\left[\ln\left(\Gamma_{w_+}(\varphi^*)\right) + \ln\left(\Gamma_{w_-}(\varphi^* - 2\pi)\right)\right] = 0 \\ \rightarrow \quad & \ln\left(1 + \beta_+ (\varphi^*)^{10} e^{\alpha_+ \varphi^*}\right) + \ln\left(1 + \beta_- (\varphi^*)^{10} e^{\alpha_- (\varphi^* - 2\pi)}\right) = 0 \vee w_1 = 0. \end{aligned}$$

This equation cannot be solved analytically and should be determined numerically. We use general parameter values as mentioned in Section 2.3. From Figure 9, three roots to this equation are expected. We find

$$\varphi_1^* \approx 0.812149, \quad \varphi_2^* \approx 3.122281, \text{ and } \quad \varphi_3^* \approx 5.410149,$$

[3]Originally we have obtained ρ_0 on the interval $[-\pi, \pi)$, but due to the cosine and tangent in the function, it is periodic and also valid on the interval $[0, 2\pi)$. Therefore, the weight dynamics can simply be written as a single integral.

to be the three roots of $q(\varphi)$. To obtain the values of φ for which $\dot{w}_2 = 0$, the roots of $q(2\pi - \varphi)$ are to be found, and are equal to $2\pi - \varphi_i^*, i = 1, 2, 3$. Now from Section 3.3.1, we know that the only stable state is equal to $\varphi^* = \arcsin(\Delta\omega/w)$. As $\Delta\omega, w \geq 0$, we know that $\varphi^* \in [0, \pi/2)$. Hence, this can only be $\varphi_1^* \in [0, \pi/2)$ for w_1 and $2\pi - \varphi_3^* \in [0, \pi/2)$ for w_1. Therefore, the nullclines are equal to the diagonal lines

$$\mu = 0 \rightarrow \begin{cases} \dot{w}_1 = 0 \iff [w_1 = 0 \quad \vee \quad w_1 + w_2 = \Delta\omega / \sin(\varphi_1^*) := \Delta\omega/\xi_1], \\ \dot{w}_2 = 0 \iff [w_2 = 0 \quad \vee \quad w_1 + w_2 = \Delta\omega / \sin(2\pi - \varphi_3^*) := \Delta\omega/\xi_2], \end{cases} \tag{16}$$

with the constants $\xi_1 \approx 0.7258, \xi_2 \approx 0.7663$.

3.4.4 Critical Points as Function of Intrinsic Frequency Difference

The phase-averaged weight evolution in the absence of noise is known in $Q := [0, 1] \times [0, 1]$ (as $w_{max} = 1$), and phase portraits can be made to determine the stability of critical points in Q. See Figure 13 for such an example, where $\vec{w} := (\dot{w}_1, \dot{w}_2)$ is the dynamic vector of unit length. The dotted line in these figures represents the transition from unstable to stable firing patterns, i.e. the line $(w_1 + w_2) = \Delta\omega$.

In this section, we illustrate how the locations of critical points move as a function of intrinsic frequency difference $\Delta\omega$. As we are mainly interested in dealing with the direction of the dynamics and not much in the size itself, only scaled dynamics are presented.

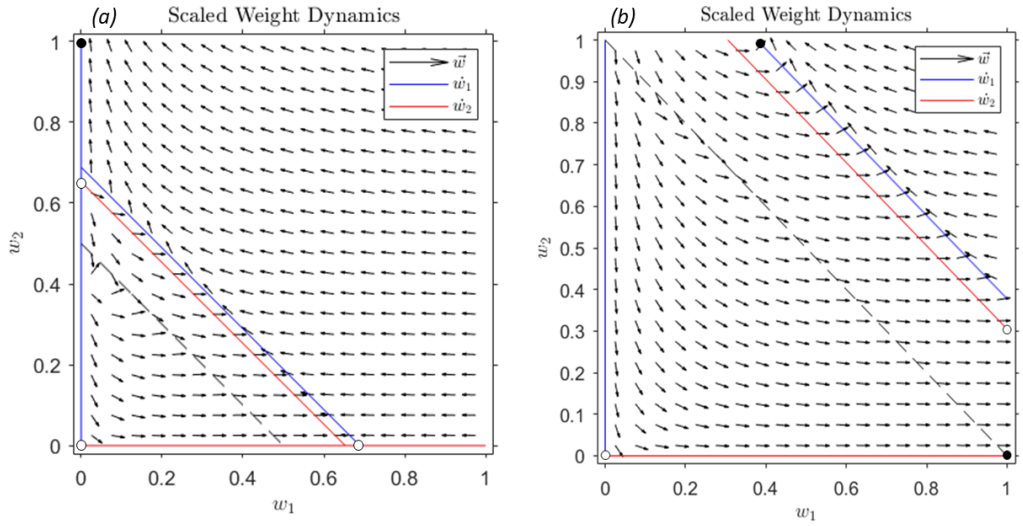

FIGURE 13: Phase portraits of the synaptic weights in the absence of noise ($\mu = 0$) with indicated nullclines and critical points (a) $\Delta\omega = 0.5$, (b) $\Delta\omega = 1.0$.

Small $\Delta\omega$

In Figure 13(a) the scaled dynamics of a relatively small intrinsic frequency difference can be seen. The nullclines are important in locating the stable weight configurations and synaptic connectivity. Note that everything above and on the right of these nullclines is moving to the left and upwards respectively. In general, the opposite happens below and on the left side of these lines. Eventually, all weights will converge to the stable point at $\lim_{t\to\infty}(w_1, w_2)(t) = (0, 1)$ for $(w_1, w_2)(0) \in (0, 1] \times (0, 1]$. However, w_1 will never actually truly reach 0 with these initial values however, due to the multiplicative update rule.

We can classify three critical points on the boundary as well. When starting with complete unidirectional coupling, bidirectional coupling can never be achieved. The three critical points are all saddle points, and equal to the intersection of the nullclines with the axes; $(0, \Delta\omega/\xi_2), (\Delta\omega/\xi_1, 0)$, together with the origin $(0, 0)$.

Increasing $\Delta\omega$

From Equation 16, it is known that increasing the value of $\Delta\omega$ will linearly increase the intersection of the nullclines with the axes. For a certain value of $\Delta\omega$, the nullclines will move past $(0, 1)$, see Figure 13(b) for such an example.

Two new stable points are created where weights can converge to. These stable configurations are $(1, 0)$ and $(\Delta\omega/\xi_1 - 1, 1)$. The initial value of the weight configuration determines the eventual stable configuration. Hitting the $w_1 = 1$ axis below the indicated saddle point implies convergence to $(1, 0)$.

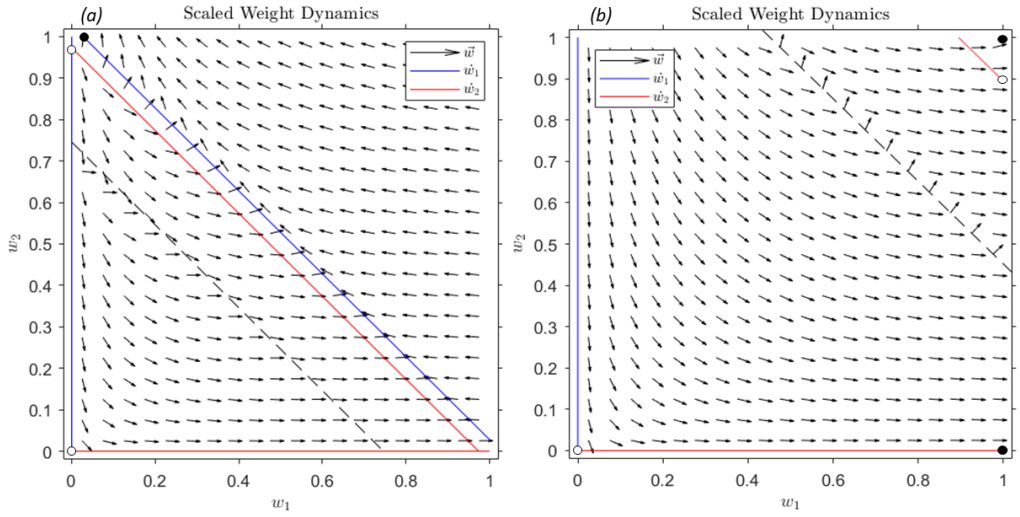

FIGURE 14: Phase portraits of the synaptic weights with indicated nullclines and critical points with $\mu = 0$. (a) $\Delta\omega = \frac{1}{2}(\xi_1 + \xi_2)$, (b) $\Delta\omega = \xi_1 + \xi_2$.

Transition case of $\Delta\omega$

The values of $\Delta\omega$ for which the two nullclines are equal to $w_1 + w_2 = 1$ are equal to $\Delta\omega = \xi_1$ and $\Delta\omega = \xi_2$. Between these values, the transition from Figure 13(a) to (b) occurs. A situation in this interval is shown in Figure 14(a). In this transition case, no critical points in the corners can be observed (except for the origin, which is always unstable).

Another transition case happens when $\Delta\omega$ increases further. For $\Delta\omega = \xi_1 + \xi_2$, the point $(1, 1)$ becomes a stable. However, this point has a small range of convergence, as most initial values will converge to $(1, 0)$. This can be seen in Figure 14(b). For larger values of the detuning frequency ($\Delta\omega > 2\xi_2$), the stable point at $(1, 1)$ disappears, and all weight configurations would simply converge to the only stable point $(1, 0)$.

All in all, the location of the critical points is summarised in Table 1. Note that for $\Delta\omega > 2$, critical points are not specified. This is due to the fact that for these values of the detuning frequency, a stable alternating firing pattern does not exist for any weight configuration and critical points are not taken into account.

TABLE 1: Overview of all critical points for different values of $\Delta\omega$.

Range of $\Delta\omega$	Stable points		Saddle points		
$(0, \xi_1]$	$(0, 1)$		$(0, 0)$,	$(0, \Delta\omega/\xi_2)$,	$(\Delta\omega/\xi_1, 0)$
$(\xi_1, \xi_2]$	$(\Delta\omega/\xi_1 - 1, 1)$		$(0, 0)$,	$(0, \Delta\omega/\xi_2)$	
$(\xi_2, 2\xi_1]$	$(\Delta\omega/\xi_1 - 1, 1)$,	$(1, 0)$	$(0, 0)$,	$(1, \Delta\omega/\xi_2 - 1)$	
$[2\xi_1, 2\xi_2]$	$(1, 1)$,	$(1, 0)$	$(0, 0)$,	$(1, \Delta\omega/\xi_2 - 1)$	
$(2\xi_2, 2)$	$(1, 0)$		$(0, 0)$		

3.4.5 Numerical Scheme for Probability Distribution Function

The location of critical points under the influence of external natural perturbations is also desired. When noise is introduced to the system, the stationary pdf ρ_s cannot be found directly using the phase difference dynamics (as could be done for $\mu = 0$. Since ρ follows the FPE as stated in Equation 14, we can determine ρ_s by solving $d\rho/dt = 0$. However, since this derivation is quite extensive as shown by [3], we will solve the FPE numerically under the assumption that it converges to a stationary distribution.

We will use the Euler-forward numerical scheme, where the interval $[0, 2\pi)$ is divided in n equally-spaced subintervals of size $\Delta\varphi := 2\pi/n$, and use time step size dt. We use the numerical scheme

$$\rho_i^{j+1} = \rho_i^j + dt\left(-\frac{\nu(\varphi_{i+1})\rho_{i+1}^j - \nu(\varphi_{i-1})\rho_{i-1}^j}{4\pi/n} + \mu\frac{\rho_{i+1}^j - 2\rho_i^j + \rho_{i-1}^j}{(2\pi/n)^2}\right), \tag{17}$$

for $i = 1, 2, \ldots n$ and $j = 0, 1, 2, \ldots$, with $\varphi_k = (k - 1/2)\,\Delta\varphi$ for $k = 0, 1, \ldots n + 1$. In our numeric scheme we have that $\rho_i^{j+1} \propto \left(1 - dt\frac{2\mu}{\Delta\varphi^2}\right)\rho_i^j$. Hence, for stability and convergence to ρ_s, it is desired that $dt < \Delta\varphi^2/2\mu$. Since we are dealing with phases, we have that $\rho(2\pi) = \rho(0)$. Therefore, the numerical derivatives can be extended along the boundaries as $\rho_{i+n}^j = \rho_i^j$ for all i. This is visualised in Figure 15(a). Equation 17 then still holds on and across the boundaries. The initial condition of the distribution is chosen to be uniform with

$$\rho_i^0 = \frac{1}{2\pi} \text{ for } i = 1, 2, \ldots n, \quad \text{such that } \sum_{i=1}^{n} \rho_i^j \Delta\varphi = 1 \text{ for all } j \geq 0.$$

The numeric scheme is run until the absolute difference between j and $j+1$ is minimal, as it is assumed we then have $\rho \approx \rho_s$. We use the smallest N for which

$$\sum_{i=1}^{n} |\rho_i^N - \rho_i^{N-1}| < \epsilon,$$

for some small $\epsilon > 0$. The steady-state probability distribution ρ_s is then approximated using the particle representation $\{\rho_i^N\}_{i=1,2,\ldots n}$, and is equal to the summation of Dirac-delta functions

$$\rho_s(\varphi) \approx \sum_{i=1}^{n} \rho_i^N \delta(\varphi - \varphi_i). \tag{18}$$

This function is still written as an approximation of the real distribution function as this is a discretisation of the continuous function. When $n, N \to \infty$ (or $\epsilon \to 0$ for the latter),

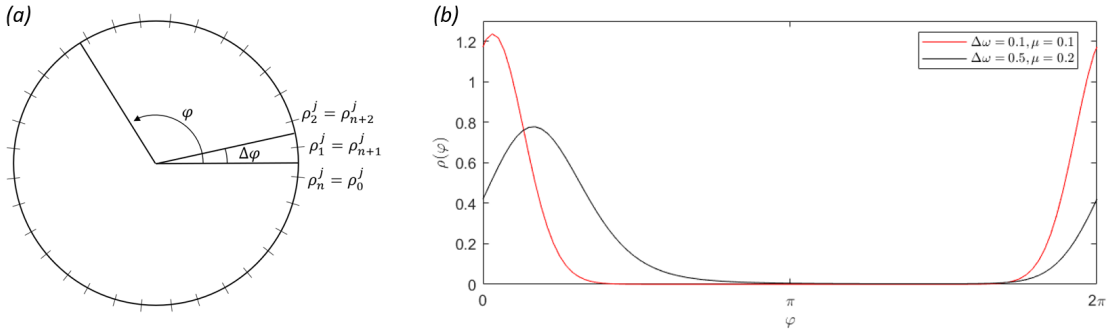

FIGURE 15: (a) Visual representation of the phase discretisation over the boundary $\varphi = 0$. (b) Examples of steady-state probability distribution function with $n = 100, \epsilon = 10^{-4}$ and $w_1 = w_2 = 0.5$. A larger intrinsic frequency differences shifts the peak of the distribution, and more noise leads to a larger spread of the distribution.

this function will approach the true continuous stationary distribution. Two examples of numerical solutions can be seen in Figure 15(b).

The stationary pdf can now be used to find the system of equations of the weights, by substituting 18 in the integral of Equation 15. For the general phase-difference-dependent update function $q(\varphi)$, we thus get

$$\mu > 0 \rightarrow \begin{cases} \dot{w_1} = w_1 \sum_{i=1}^{n} \rho_i^N q(\varphi_i), \\ \dot{w_2} = w_2 \sum_{i=1}^{n} \rho_i^N q(2\pi - \varphi_i). \end{cases}$$

This numerical method can be applied to the complete domain Q. Again for $w < \Delta\omega$, the phase difference does not converge to a stable state, regardless of the added noise. Nevertheless, the probability density function can still be found numerically in this region.

3.5 Bifurcation Diagrams and Stable Synaptic Connectivity

As seen earlier in Section 3.4.4, the location of stable weight configurations depends on parameter values, and can be determined in the absence of noise. However, when noise is introduced to the system, the dynamics become even more complex. Therefore, this is analysed numerically using a bisection method on the corners of Q. All in all, the locations of stable points are summarised in Figures 16 and 17. These bifurcation diagrams only show the behaviour for $\Delta\omega \leq 2$, as for larger values, no stable phase difference solution exists for all values of w_1, w_2, and the assumption of alternating firing pattern in invalid. Critical lines are found by applying the bisection method, fixing $\Delta\omega$ and interpolating μ until an accurate approximation is found where either $\dot{w_1}$ or $\dot{w_2}$ is equal to zero on a corner of the domain Q. On the axis $\mu = 0$, the theoretical found values from Section 3.4.4 are used. On one side of the critical lines, the weight configurations are unstable, while on the other side they are stable. This depends on both values of $\dot{w_1}$ or $\dot{w_2}$. For instance, the weight configuration $(1, 1)$ is stable if and only if $\dot{w_1} > 0$ and $\dot{w_2} > 0$ at $(1, 1)$.

Since nullclines are always diagonals where $w_1 + w_2$ is constant, the critical lines for the diagonal $w_1 + w_2 = 1$ are shown (red), which applies for both corners $(1, 0)$ and $(0, 1)$. It is interesting to note how for $w_1 + w_2 = 2$ (black) all lines scale linearly compared to the red critical lines.

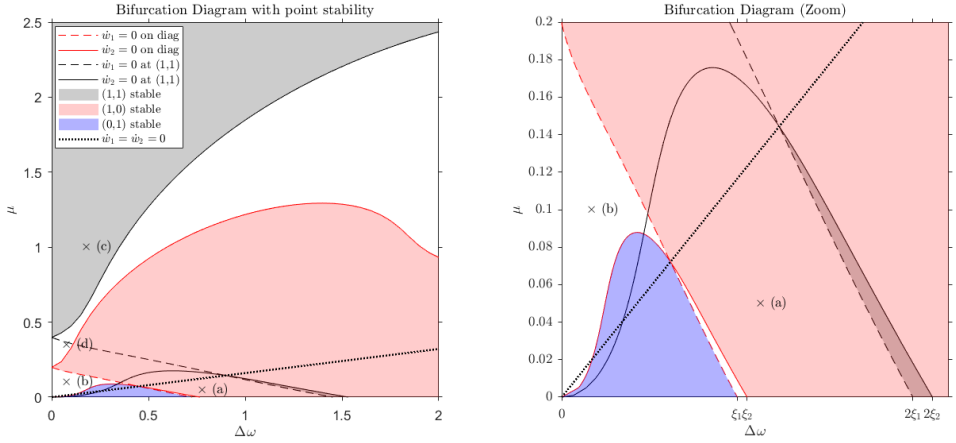

FIGURE 16: Bifurcation diagrams with stability of the corners in the weight range.

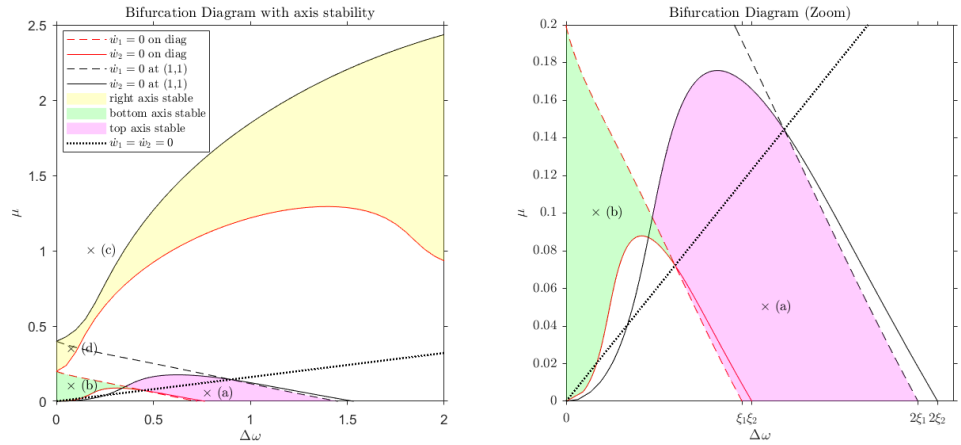

FIGURE 17: Bifurcation diagrams with indicated stability on the axes in the weight range.

From Equation 16 it became clear that the nullcline $\dot{w}_1 = 0$ always lies above the nullcline of w_2 when $\mu = 0$. This resulted in the critical points of the weight configurations lying on the boundaries of Q. However, when noise is introduced, the order of these nullclines can reverse. Therefore, since the weight dynamics is a continuous function of the parameter values, there exist parameter values for which the nullclines are equal. This implies there is a complete straight line $w_1 + w_2 \in (0, 2)$, for which $\dot{w}_1 = \dot{w}_2 = 0$. On this line, all weight configurations are stable. This turns out to be for the parameter values

$$\mathcal{C} := \frac{\Delta\omega}{\mu} = 0.16053,$$

and is shown with the dotted black line in both bifurcation diagrams. This line is the intersection of the two critical lines for $\dot{w}_1$ and $\dot{w}_2$.

In Figure 17, the stability of three axes are shown. This implies that there is stability on a single point (with exception of the corners) on the axis itself and not the full axis. There are two critical lines for $\dot{w}_2 = 0$ at the corners of Q, implying there is the possibility to have two nullclines for w_2, something that cannot be seen in the case $\mu = 0$. Examples of interesting weight dynamics are discussed in the next Section 3.5.1.

3.5.1 Phase Portraits and Nullclines with Noise

For different parameter values phase portraits are shown for the coupling weights in Figure 18(a-d). These figures correspond to the letters (a-d) indicated in the bifurcation diagrams (Figures 16 and 17).

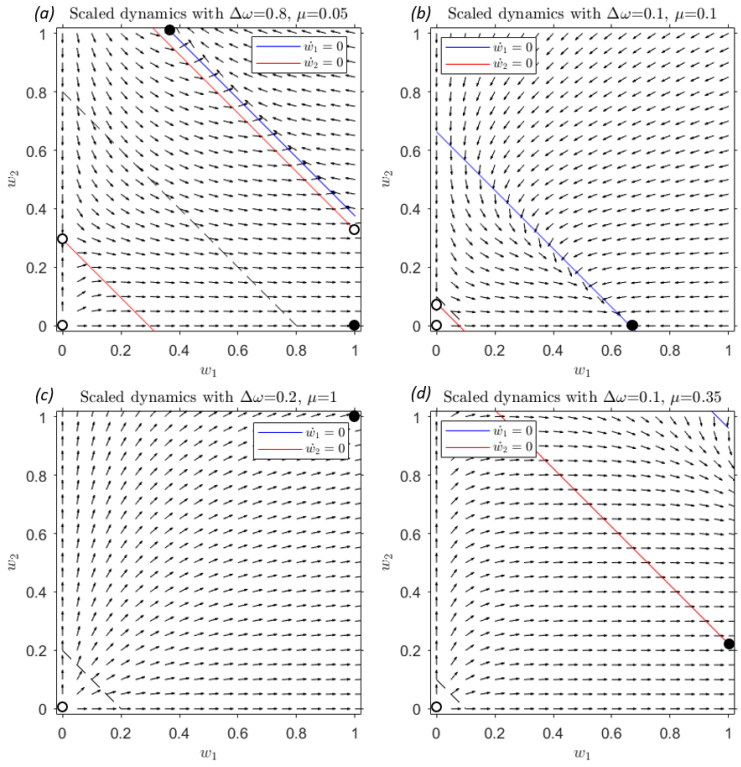

FIGURE 18: Weight phase portraits with nullclines and critical points in four different locations as indicated in the bifurcation diagrams.

Nullclines have been indicated in the phase portraits. These are found by using the bisection method, approximating roots of the derivatives at the places $w_1 = 0.05, 0.50, 0.95$ while varying w_2. This interval-halving method is performed 16 times to the interval to $[0, 1]$ to obtain an accuracy of $1.5 \cdot 10^{-5}$. For a single nullcline, this only has to be done for one value of w_1 as nullclines always lie directly diagonal with slope -1 as mentioned before. This is in general true for all odd coupling functions g, as in that case the function $\nu(\varphi)$ always depends on the summation of weights $w_1 + w_2$. Consequently, the nullclines of w_1 and w_2 consist of diagonals where the value of $w_1 + w_2$ is constant. As a result, if a fixed point (w_1^*, w_2^*) as found by the bisection method exists in Q, it leads to a nullcline of fixed points corresponding to the straight line $w_1 + w_2 = w_1^* + w_2^*$.

Critical points are indicated using the intersection of nullclines with boundaries of Q. In Figure 18(a) we observe bistability of weight configurations in Q, both unidirectional coupling $(1, 0)$ and weak bidirectional coupling $(0.4, 1)$ are stable. This is in line with both bifurcation diagrams, as point (a) lies in both respective regions. Moreover, a third nullcline has been added, creating another saddle point. Figure 18(b) and (d) shows stability on the bottom and right axis respectively, something not possible for $\mu = 0$.

In Figure 18(c) no nullclines are visible, even though $\Delta\omega = 0.2$ is relatively small. We conclude that large values of noise results in stable bidirectional coupling of the neurons, with a stable firing pattern.

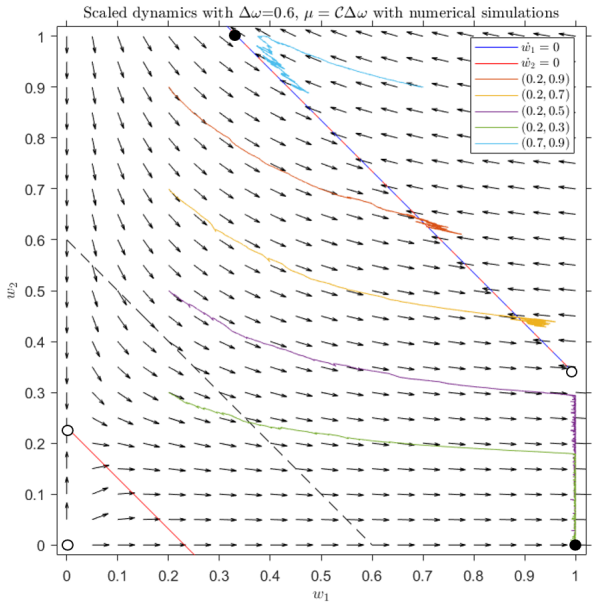

FIGURE 19: Phase portrait with five numerical simulations from different initial conditions showing the stability inside Q, with $\mu = \mathcal{C}\Delta\omega$. Since the magnitude of the weight dynamics is very small around the nullclines, the influence of noise is large and weight configurations will move around without stabilising into a single configuration. It can be seen that the of $\dot{w}_1$ is especially larger around the nullclines.

Figure 19 shows a critical phase portrait. Here, the diagonal nullcline through the domain is entirely stable. Depending on the initial value, the weight configuration will stabilise around this diagonal, or converge to the stable weight configuration $(1, 0)$. Note that a point on the top axis is still also a stable point, corresponding with the location of this critical parameter value configuration in Figures 16 and 17. In- or decreasing μ slightly will remove the mid-domain stability, but keep stability on the top axis and $(1, 0)$.

3.6 Comparison with LIF

The phase difference model has been developed after the leaky integrate-and-fire model to simplify analysis. The two should describe the same kind of weight stability. Therefore, we will compare the results from Figure 6 and Figures 16 and 17. These results cannot be compared directly and linearly. Firstly, the LIF model describes the membrane potentials V_i that are influenced by input intensities I_i. A difference in input ΔI cannot be related directly to difference in intrinsic frequency $\Delta\omega$. Note, however, that increasing ΔI is similar to increasing $\Delta\omega$. Secondly, the noise intensity is equal to σ and $\sqrt{\mu}$ respectively. However, these can also not be scaled (also not quadratically), as a perturbation on the membrane potential V is not directly the same as a perturbation on the phase difference. Again, we note that increasing σ is equivalent to increasing μ.

From the LIF model, we concluded that for small difference in natural frequencies and small additive noise, unidirectional coupling with $(w_1, w_2) = (0, 1)$ is stable. The same can be concluded for the phase model from Figure 16. Moreover, increasing the input intensity difference resulted in a switch of the type of unidirectional coupling from $(0, 1) \to (1, 0)$. This is also a result by Figures 16 and 17, where bistability exists with $(1, 0)$ being stable. A point on the top axis $(\cdot, 1)$ is also stable in the phase difference model, something that can be recognised in the right hand side of Figure 5.

4 Discussion

In the first part of the paper, we developed a leaky integrate-and-fire model with STDP for inhibitory neurons. Since the LIF model is not able to reproduce all fundamental properties of cortical spiking neurons, results might not be biophysically accuracte [2]. However, due to the linearity, computational speed, and comparison with the phase-difference model, it provides a decent framework for mathematical analysis. Results depend on many model parameters, changing $\alpha, \varrho, \Delta I$, and initial conditions will directly influence the final states of the weight configurations and firing patterns. Input parameters α and ϱ are chosen such that suppression is eliminated for a wide range of ΔI, but this coupling could be unrealistically low. The possibility exists that the de-synchronisation induced by ΔI is too large, and that smaller values with larger values for coupling intensity ϱ should be used. Moreover, it was expected that weight configurations would stabilise, irrespective of initial weight conditions. However, for large initial weight values, immediate suppression occurred. Results are therefore only interpreted for weak initial bidirectional coupling.

In the second part of the paper, a phase difference model is developed to approximate the LIF model more generally. This model is less dependent on choice of parameter values, as the dynamics of two neurons is described by a single stochastic differential equation. This highly simplifies analysis, but also simplifies the extent to which results are applicable to the initial LIF model. For instance, only the intrinsic frequency difference $\Delta\omega = \omega_2 - \omega_1$ is used, irrespective of the original values. What could be seen in the LIF model is that the dynamics is largely dependent on both I_1 and I_2 and not just the difference ΔI. It is to be expected that the same applies to the frequency detuning $\Delta\omega$, however, analysis is independent of the separate frequencies which could miss out on fundamental properties.

A new framework has been developed, such that PDDP can be used to study multiplicative learning rules, extending the framework of the scientific field. The fundamental assumption of this transformation is the presence of an alternating firing pattern, which can only be reached for small $\Delta\omega/\Omega$. Since inhibition causes synchronization in coupled neurons as shown by [9], this might be a valid assumption for a large range of parameter values. On top of that, when determining the phase-averaged weight dynamics using the Fokker-Planck equation, it is assumed that the coupling dynamics have to be slow enough to render valid averaging of the FPE. From the LIF model it can be seen that this assumption is generally valid. To ensure truly slower dynamics, larger values of n Could be used. Under both assumptions, we have developed a technique that can be generally applied to multiplicative STDP functions.

The PDDP model yields qualitatively equivalent results to the STDP model. However, there are some features that might not be captured by the phase difference model, as the firing pattern of two neurons is described by one stochastic differential equation. Again, using only the difference in firing frequency $\Delta\omega$ forms an example of this.

The phase difference model is developed to model coupled inhibitory neurons. However, this inhibitory coupling does not come into play directly as coupling is described by the periodic coupling function g, which does not use inhibition as directly as the LIF model. Inhibition is mainly included in the choice of learning rule, which is specifically found for inhibitory neurons. It is important to note that analysis is performed only for sinusoidal coupling with $g(\varphi) = \sin(\varphi)$, but can be extended to other coupling functions as well. This will change the stable firing phase difference φ^* and might induce multi-stability of the phase difference. The stationary pdf ρ_s will change in that case, which will change the overall phase-averaged weight dynamics. Nullclines will remain straight lines with slope -1 for odd coupling functions (and 1 for even functions).

Results of the LIF model show that both unidirectional coupling and bidirectional coupling can be stable types of synaptic connectivity. Bistability of coupling configurations was not found as suppression often occurred for large initial weight conditions. Large values of additive noise resulted in chaotic weight behaviour, where weak bidirectional coupling is often stable. Decoupling of the neurons was not observed and can be seen as unstable. The phase difference model shows similar results as the LIF model, where unidirectional coupling was stable for small difference in intrinsic frequency. Multi-stability of weight configurations could be observed for a large range of parameter values, with unidirectional and weak bidirectional coupling being the main stable types of synaptic connectivity. Similar to findings from the LIF model, neuron decoupling is always unstable. For small $\Delta\omega$, weight configurations will always converge to a state where the phase difference stabilises and the neurons synchronise.

Future work can be done for investigating different coupling functions g, which can demonstrate the connection between the LIF and phase difference more clearly. Moreover, the mathematical connection between the variables σ, μ and $\Delta I, \Delta\omega$ is important to relate the two respective models directly. On top of that, the basin of attraction of stable weight configurations could be explored, as bistability of weak bidirectional and unidirectional coupling occurs for a large range of parameter values. The final state of the weight configuration can be predicted based on its initial condition, taking additive noise into account. Lastly, only one learning rule is explored, while more learning rules for inhibitory neurons are known as provided by [5], which could be explored further.

5 Conclusion

All in all, for small difference in natural firing frequency and low additive noise, the phase difference model is a good representation of the leaky integrate-and-fire model. For large values of $\Delta\omega$, the assumption of alternating firing pattern does not hold as a stable phase difference does not exist, and strong conclusions cannot be drawn.

By switching from additive to multiplicative STDP, and by modifying the learning rule to one applicable to inhibitory neurons, completely different dynamics appear compared to the results shown by [3], where stability only appeared on the corners of Q and decoupling was only stable. This indicates the complexity of the phase-difference model and the potential for further research, using different learning rules and coupling functions.

For coupled inhibitory neurons with synaptic weights following STDP, multi-stability is possible with unidirectional and bidirectional coupling, both weak and strong. Unidirectional coupling is significantly more stable compared to strong bidirectional coupling, as the basin of attraction is small for the latter in the case of bistability. Lastly, we have shown that stability exists inside the domain Q when nullclines overlap. This implies that due to natural perturbations, weight configurations can remain dynamic over time on this line and synaptic connectivity remains dynamic.

We conclude that decoupling for inhibitory neurons is unstable and that weight configurations will always converge to stable unidirectional or (weak) bidirectional coupling. Since decoupling is unstable, the sum of weights will always be sufficiently large to induce a synchronised firing pattern. A stable state on the bottom axis close to decoupling can be achieved using very small $\Delta\omega$, and by introducing some additive noise, but this can never be achieved in the absence of noise. True unidirectional coupling is stable for a large range of values of external perturbations. For significantly large values ($\mu > 2$), strong bidirectional coupling is the only stable synaptic connectivity.

References

[1] Julie S Haas, Thomas Nowotny, and Henry DI Abarbanel. Spike-timing-dependent plasticity of inhibitory synapses in the entorhinal cortex. *Journal of neurophysiology*, 96(6):3305–3313, 2006.

[2] Eugene M Izhikevich. Which model to use for cortical spiking neurons? *IEEE transactions on neural networks*, 15(5):1063–1070, 2004.

[3] Leonhard Lücken, Oleksandr V Popovych, Peter A Tass, and Serhiy Yanchuk. Noise-enhanced coupling between two oscillators with long-term plasticity. *Physical Review E*, 93(3):032210, 2016.

[4] Constantine A Mangina and Evgeni N Sokolov. Neuronal plasticity in memory and learning abilities: Theoretical position and selective review. *International Journal of Psychophysiology*, 60(3):203–214, 2006.

[5] Kazushi Murakoshi and Kyoji Suganuma. A neural circuit model forming semantic network with exception using spike-timing-dependent plasticity of inhibitory synapses. *Biosystems*, 90(3):903–910, 2007.

[6] José A Obeso, Maria C Rodriguez-Oroz, Manuel Rodriguez, José L Lanciego, Julio Artieda, Nancy Gonzalo, and C Warren Olanow. Pathophysiology of the basal ganglia in parkinson's disease. *Trends in neurosciences*, 23:S8–S19, 2000.

[7] Jonathan Rubin, Daniel D Lee, and H Sompolinsky. Equilibrium properties of temporally asymmetric hebbian plasticity. *Physical review letters*, 86(2):364, 2001.

[8] Mark CW Van Rossum, Guo Qiang Bi, and Gina G Turrigiano. Stable hebbian learning from spike timing-dependent plasticity. *Journal of neuroscience*, 20(23):8812–8821, 2000.

[9] Carl Van Vreeswijk, LF Abbott, and G Bard Ermentrout. When inhibition not excitation synchronizes neural firing. *Journal of computational neuroscience*, 1(4):313–321, 1994.

[10] Jerrold L Vitek. Deep brain stimulation for Parkinson's disease. *Stereotactic and functional neurosurgery*, 78(3-4):119–131, 2002.

[11] Jerrold L Vitek, Takao Hashimoto, John Peoples, Mahlon R DeLong, and Roy AE Bakay. Acute stimulation in the external segment of the globus pallidus improves parkinsonian motor signs. *Movement disorders: official journal of the Movement Disorder Society*, 19(8):907–915, 2004.

A Appendix: Figures

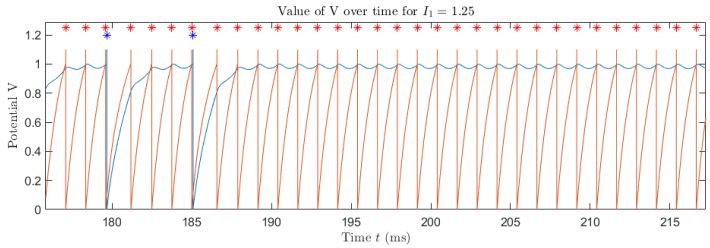

FIGURE 20: Numerical simulations with $\varrho = 0.40$ and $w_1(0) = w_2(0) = 0.5$. In this part of the simulation synaptic weights are not significantly large ($w_1 \approx 0.8, w_2 \approx 0.65$). However, due to the large value of connectivity strength ϱ, neuron 2 is completely suppressed.

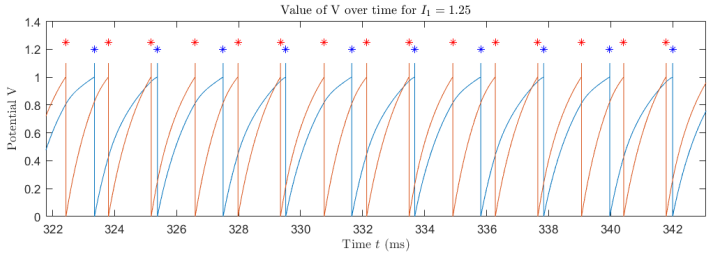

FIGURE 21: Numerical simulations with $\varrho = 0.15$ and $w_1(0) = w_2(0) = 0.2$. In this part of the simulation synaptic weights are large ($w_1 \approx w_2 \approx 0.95$) and connectivity should be significant. However, due to the low value of connectivity strength ϱ, the influence of the coupling is negligible. Membrane potentials simply follow their natural frequency.

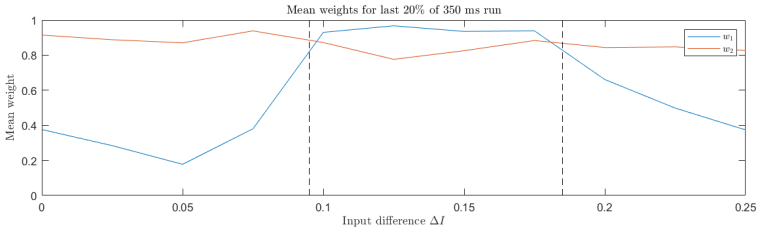

FIGURE 22: Average weights after a long run as a function of input difference ΔI, with $\varrho = 0.2, w_1(0) = 0.2, w_2(0) = 0.8$. Note the three intervals for which unidirectional and bidirectional coupling is stable. The intervals of synaptic connectivity are separated by the values $\Delta I = 0.095$ and $\Delta I = 0.185$.

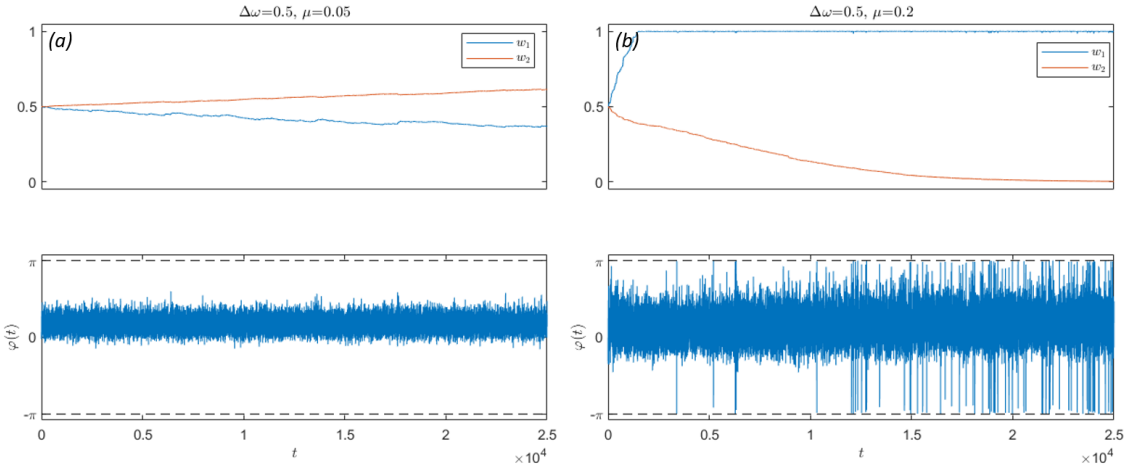

FIGURE 23: Numerical simulations with $\Delta\omega = 0.5$ and $w_1(0) = w_2(0) = 0.5$. Note only the phase dynamics depends on the noise intensity, but also the final weight configuration changes. (a) $\mu = 0.05$. (b) $\mu = 0.2$.

B Appendix: Equations

B.1 STDP to PDDP

The transformation from STDP to PDDP is obtained as follows

$$\begin{aligned}
\frac{dw_1(t)}{dt} &= \lim_{dt\to 0} \frac{w_1(t+dt) - w_1(t)}{dt} = \lim_{dt\to 0} \frac{\left(\left(\Gamma_{w_1}\right)^{dt\Omega/2\pi} - 1\right) w_1(t)}{dt} \\
&\approx \lim_{dt\to 0} \frac{\left(\left(\left(\Gamma_{w_+}(\Delta t_2)\cdot\Gamma_{w_-}(-\Delta t_1)\right)^{\Omega/2\pi}\right)^{dt} - 1\right)}{dt} w_1(t) \\
(*) &= \ln\left(\left(\Gamma_{w_+}(\Delta t_2)\cdot\Gamma_{w_-}(-\Delta t_1)\right)^{\frac{\Omega}{2\pi}}\right) w_1(t) \\
&= \frac{\Omega}{2\pi}\left[\ln\left(\Gamma_{w_+}(\Delta t_2)\right) + \ln\left(\Gamma_{w_-}(-\Delta t_1)\right)\right] w_1(t) \\
&\approx \frac{\Omega}{2\pi}\left[\ln\left(\Gamma_{w_+}\left(\frac{\varphi}{\Omega}\right)\right) + \ln\left(\Gamma_{w_-}\left(\frac{\varphi - 2\pi}{\Omega}\right)\right)\right] w_1(t),
\end{aligned} \tag{19}$$

where step $(*)$ is done by applying l'Hôpital's rule. For neuron 2 the same analysis can be performed, since the roles from the spike-timing differences is directly reversed with

$$w_2(t+dt) \approx w_2(t)\cdot\left(\Gamma_{w_+}(\Delta t_1)\cdot\Gamma_{w_-}(-\Delta t_2)\right)^{dt\Omega/2\pi}.$$

Therefore,

$$\begin{aligned}
\frac{dw_2(t)}{dt} &= \lim_{dt\to 0} \frac{w_2(t+dt) - w_2(t)}{dt} \\
&\approx \lim_{dt\to 0} \frac{\left(\left(\left(\Gamma_{w_+}(\Delta t_1)\cdot\Gamma_{w_-}(-\Delta t_2)\right)^{\Omega/2\pi}\right)^{dt} - 1\right)}{dt} w_2(t) \\
&= \ln\left(\left(\Gamma_{w_+}(\Delta t_1)\cdot\Gamma_{w_-}(-\Delta t_2)\right)^{\frac{\Omega}{2\pi}}\right) w_2(t) \\
&= \frac{\Omega}{2\pi}\left[\ln\left(\Gamma_{w_+}(\Delta t_1)\right) + \ln\left(\Gamma_{w_-}(-\Delta t_2)\right)\right] w_2(t) \\
&\approx \frac{\Omega}{2\pi}\left[\ln\left(\Gamma_{w_+}\left(\frac{2\pi-\varphi}{\Omega}\right)\right) + \ln\left(\Gamma_{w_-}\left(-\frac{\varphi}{\Omega}\right)\right)\right] w_2(t) \\
&= q(2\pi-\varphi)w_2(t)
\end{aligned} \tag{20}$$

B.2 Numerical Schemes

Numerical Scheme for LIF model
Using Euler-Maruyama with timestep-size dt, $k = 0, 1, 2, \ldots$, and $t_k := k \cdot dt$, we obtain the numerical scheme

$$\begin{cases} V_1^{k+1} = V_1^k + dt\left(-V_1^k + I_1(t_k)\right) + \sigma\sqrt{dt}\eta_1, \\ V_2^{k+1} = V_2^k + dt\left(-V_2^k + I_2(t_k)\right) + \sigma\sqrt{dt}\eta_2, \end{cases} \qquad \text{where } \eta_1, \eta_2 \sim N(0,1). \tag{21}$$

Numerical Scheme for Phase Model
Using Euler-Maruyama with timestep-size dt, and $k = 0, 1, 2, \ldots$ we obtain the numerical scheme

$$\begin{cases} \varphi^{k+1} = \left[\varphi^k + dt\left(\Delta\omega + w_2^k g(-\varphi^k) - w_2^k g(\varphi^k)\right) + \eta\sqrt{2\mu\cdot dt}\right] \mod 2\pi \\ w_1^{k+1} = \min\left(w_1^k + dt\cdot w_1^k q(\varphi^k), 1\right), \\ w_2^{k+1} = \min\left(w_2^k + dt\cdot w_2^k q(2\pi-\varphi^k), 1\right), \end{cases} \tag{22}$$

where again, $\eta \sim N(0,1)$. For the phase difference, $\mod 2\pi$ is required as $\varphi \in [0, 2\pi)$. Hard bounds on the weights are put by the minimum functions as $w_i \leq w_max$, weights cannot exceed the maximum $w_{max} = 1$. Weights can also not exceed the minimum 0. However, we cannot equal the weight to 0 when it does exceed as this limit, as this can never truly happen. Therefore, if the weight value as in Equation 22 does come below 0, the value is reset equal to half to its previous value:

$$\text{if } w_i^{k+1} < 0 \to w_i^{k+1} = w_i^k/2.$$